Quantum treatment of phonon scattering for modeling of three-dimensional atomistic transport

Y. Lee,[1,*] M. Bescond,[1,†] N. Cavassilas,[1] D. Logoteta,[1] L. Raymond,[1] M. Lannoo,[1] and M. Luisier[2]

[1]*IM2NP, UMR CNRS 7334, Aix-Marseille Université, Technopôle de Château-Gombert, Bâtiment Néel,*
60 Rue Frédéric Joliot Curie, 13453 Marseille, France
[2]*Integrated Systems Laboratory, ETH Zürich, 8092 Zürich, Switzerland*

Based on the nonequilibrium Green's function formalism, we show a numerically efficient method to treat inelastic scattering in multidimensional atomistic codes. Using a simple rescaling approach, we detail the calculations of the lowest-order approximation (LOA) [Y. Lee *et al.*, Phys. Rev. B **93**, 205411 (2016)] series to the usual, computationally intensive, self-consistent Born approximation (SCBA). This, combined with the analytic continuation technique of Padé approximants, is applied to an atomistic code based on a tight-binding $sp^3d^5s^*$ model for electrons and holes, and a modified valence-force-field method for phonons. Currents in Si and Ge gate-all-around nanowire transistors are then computed considering the main crystallographic transport directions ($\langle 100 \rangle$, $\langle 110 \rangle$, $\langle 111 \rangle$) for both *n*-type and *p*-type devices. Our results show that in most configurations, third-order LOA currents are enough to achieve a high agreement with SCBA results, while reducing the calculation time by about one order. In addition, we propose a criterion to determine the validity of such expansion techniques.

The recent introduction of three-dimensional (3D) fin structured trigate transistors in the semiconductor industry has opened the door for a steady continuation of Moore's scaling law in the sub-20 nm technology node [1]. However, despite the success of the device architecture for the mass production, there is a remaining question: Will this device structure still be valid for transistors with sub-10 nm gate lengths? In this perspective, the ongoing research mainly focuses on (i) improving the electrostatic control of the device architecture like gate-all-around (GAA) Si nanowire [2], or (ii) searching novel materials exhibiting high mobilities and/or high band gap [3–8], or (iii) the combination of both aspects, like wrap-gated InGaAs III-V nanowire transistors [9–11].

In all the aforementioned devices both theoretical [12–15] and experimental [16] works underline the impact of the position of each individual atom on the obtained performance. Indeed, the physics of nanoscaled devices is mainly governed by quantum effects (confinement [17] and tunneling [18,19]), surface roughness scattering [20], and electron-phonon interactions [21]. Among those phenomena, it has been theoretically predicted [8,22] that inelastic interactions between electrons and phonons play a major role even in ultrascaled devices with dimensions of the order of the electron mean free path. Thus, in order to analyze the physical properties of the devices, the development of atomistic quantum simulation tools including inelastic electron-phonon scattering is urgently needed. During recent decades, several quantum methods have been proposed to treat this issue precisely. Among them the nonequilibrium Green's function (NEGF) formalism [23–25] is one of the most advanced quantum methods that has attracted intensive interests due to its suitability for addressing inelastic carrier transport in nanostructures.

Unfortunately, atomistic NEGF quantum transport simulations of realistic devices require important numerical resources. The situation becomes even more complicated when inelastic interactions are included. Indeed, phonon scattering is usually treated with the self-consistent Born approximation (SCBA) that induces an additional self-consistent scheme to the conventional "Poisson-Schrödinger" loop. The SCBA was first applied to simple effective mass or $\mathbf{k} \cdot \mathbf{p}$ Hamiltonians [26,27]. It was then implemented in 3D full-band atomistic NEGF codes based on the tight-binding Hamiltonian [21,28]. Among those advanced codes, the simulator OMEN developed by Luisier and co-workers is one of the most sophisticated that couples inelastic transport of phonons and electrons with an atomistic precision [29,30]. However, this simulator is only manageable with more than 1000 CPUs due to unavoidable numerical burden.

Recently, we proposed a technique that allows one to greatly reduce the computational complexity for taking into account the interaction between electrons and phonons within the NEGF framework. The approach [31–33] is based on a lowest-order approximation (LOA) of the interactions combined with an analytic continuation technique of Padé approximants [34,35]. Its main advantage is to avoid the numerous iterations required by SCBA. However, it implies the inversions and multiplications of potentially large matrices which may be impractical for 3D systems. We here present a simple rescaling technique able to calculate a series of LOAs using the first iterations of the conventional SCBA algorithm. We apply this efficient technique to the atomistic code OMEN [29] to model 3D nanowire (NW) transistors for which electron-phonon scattering is important. In particular, we show that the physical quantities (i.e. the currents) based on the third-order LOA combined with the Padé analytic continuation technique are enough to obtain the results of the full SCBA iterations. Our investigations focus on both *n*-type and *p*-type Si GAA NWs considering the three main crystallographic orientations ($\langle 100 \rangle, \langle 110 \rangle, \langle 111 \rangle$). Application to a Ge NW in $\langle 110 \rangle$ transport direction is also discussed.

The device structure investigated in this Rapid Communication is schematized in Fig. 1. The chosen gate length is 5 nm

---
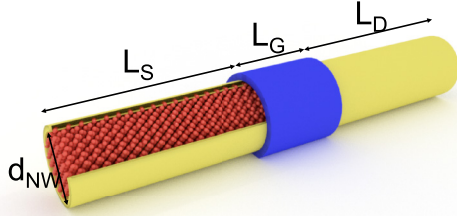*youseung.lee@im2np.fr
†marc.bescond@im2np.fr

FIG. 1. Schematic representation of the silicon GAA NW transistors considered in this work (with a $\langle 100 \rangle$ crystallographic orientation in the present case). The length of the gate is $L_G = 5$ nm, the source and drain extensions $L_{S/D} = 15$ nm, and the diameter of NW $d_{\mathrm{NW}} = 3$ nm. Source and drain regions are doped with a doping concentration of donors or acceptors $N_{D/A} = 1 \times 10^{20}$ cm^{-3}. Si$\langle 110 \rangle$, Si$\langle 111 \rangle$, and Ge$\langle 110 \rangle$ are also considered (not shown).

since it is considered as an ultimate limit for conventional logic transistors. The channel is surrounded by a 3-nm-thick HfO$_2$ dielectric layer (with $\epsilon_R = 20$), while source and drain regions are covered by a low κ dielectric layer (with $\epsilon_R = 5$). A supply voltage $|V_{DS}| = |V_{DD}| = 0.6$ V is applied between the source and drain contacts, and a gate-to-source bias V_{GS} then controls the currents flowing inside the channel. Since electron-phonon scattering is found to be stronger in the saturation regime [21], we focus here on this operation mode.

We consider steady-state electron transport described within the NEGF framework employing a full-band tight-binding $sp^3 d^5 s^*$ model without spin-orbit coupling [36,37]. The lateral surface of the semiconductor NW in which we solve the Schrödinger's equation is passivated by increasing the energy of dangling bonds [38], and no surface roughness scattering is considered. Phonon relation dispersion in the confined NW is obtained via a modified valence-force-field method including four interaction terms [39,40]. Here, as described in Ref. [29], electrons are coupled to phonons through the following diagonal lesser or greater self-energy:

$$
\Sigma_{nn}^{\lessgtr \sigma_1 \sigma_2}(E) = i \sum_l \sum_{ij} \sum_{\sigma_3 \sigma_4} \int_{-\infty}^{\infty} \frac{d(\hbar w)}{2\pi} \nabla_i H_{nl}^{\sigma_1 \sigma_3}
$$
$$
\times G_{ll}^{\lessgtr \sigma_3 \sigma_4}(E \mp \hbar \omega) \nabla_j H_{ln}^{\sigma_4 \sigma_2} \big[D_{ln}^{\lessgtr ij}(\omega)
$$
$$
- D_{ll}^{\lessgtr ij}(\omega) - D_{nn}^{\lessgtr ij}(\omega) + D_{nl}^{\lessgtr ij}(\omega) \big], \quad (1)
$$

where $\hbar$ is the reduced Planck's constant, E the electron energy, ω the phonon frequency, H_{nl} the Hamiltonian (tight-binding matrix element), $G(E)$ the electron Green's function, and $D(\omega)$ the phonon Green's function expressed in the real space (the indices i and j run over x, y, and z directions). The other indices n and l denote all atomic positions, and σ represents the orbitals. $\nabla_i H_{nl}$ represents the first derivative of the tight-binding Hamiltonian matrix H_{nl} along the i direction (x, y, or z). It defines the electron-phonon coupling due to atom oscillations around their equilibrium position (please see Ref. [29] for more details). We assume a bath of phonons at thermal equilibrium by considering no temperature gradients inside the device and by neglecting the phonon self-energies

which can contribute to the phonon Green's function $D(\omega)$ (see Ref. [29]). We should note that the diagonal approximation of the self-energy, which results from computational limitations in atomistic codes, may lead to an underestimation of the strength of electron-phonon coupling [41,42]. However, Ref. [43] showed that the diagonal approximation was still valid in ultrascaled Si nanowires for electrons, except for transport along the $\langle 110 \rangle$ crystal orientation. More generally, the LOA combined with the Padé approximant can be applied to nondiagonal self-energies. The self-energy of Eq. (1) combined with Dyson's equation [44] allows one to calculate the electron interacting Green's function $G(E)$ starting from the noninteracting one $g(E)$.

$$
G = g + g \Sigma[G] G, \quad (2)
$$

where the simplified matrix notation $[1 = (r_1, t_1), g \Sigma[G] G = \int d2 \int d2'\, g(1;2) \Sigma(2;2') G(2';1')]$ is used. Dyson's equation (2) is typically solved using the so-called iterative SCBA scheme with a specified convergence tolerance such as

$$
G_N = \{ g^{-1} - \Sigma[G_{N-1}] \}^{-1}, \quad (3)
$$

where G_N is the Green's function at the Nth SCBA iteration and $G_0 = g$.

Green's functions resulting from the first few iterations [i.e., N small in Eq. (3)] of the SCBA scheme are generally not conserving for strong electron-phonon interactions [31,33]. The SCBA might then require more than several dozens of iterations to provide accurate conserving physical properties. On the other hand, LOA Green's functions are conserving at any order. It has been shown that the first few orders of LOA Green's functions coupled with Padé approximants can highly accelerate the calculations of physical quantities (both current and charge density) [31]. However, the LOA Green's function algorithm presented in Ref. [31] implies numerous inversions and multiplications of Green's function matrices. Its implementation is then numerically very demanding when applied to 3D nanostructures. Here, we show that the derivation of LOA Green's functions from the usual SCBA algorithm can be easily reached by introducing a scaling parameter to Eq. (1).

As an example, let us rewrite Eq. (3) in the Taylor series expansion as

$$
G_N = g + g \Sigma[G_{N-1}] g + g \Sigma[G_{N-1}] g \Sigma[G_{N-1}] g + \cdots.
$$
$$(4)$$

The first SCBA Green's function G_1 is then defined from Eq. (4) as

$$
G_1 = g + g \Sigma[g] g + g \Sigma[g] g \Sigma[g] g + \cdots. \quad (5)
$$

G_1 is not conserving due to second- and higher-order terms in interaction [33]. Its first-order LOA counterpart G_{LOA1} is conserving and expressed as

$$
G_{\mathrm{LOA1}} = g + g \Sigma[g] g. \quad (6)
$$

G_{LOA1} can then be deduced from G_1 by introducing a scaling parameter $1/\lambda_1$ in the self-energy of Eq. (1). G_1 rescaled by λ_1 is now defined by

$$
G_1^{\lambda_1} = g + \frac{1}{\lambda_1} g \Sigma[g] g + \left(\frac{1}{\lambda_1} \right)^2 g \Sigma[g] g \Sigma[g] g + \cdots. \quad (7)
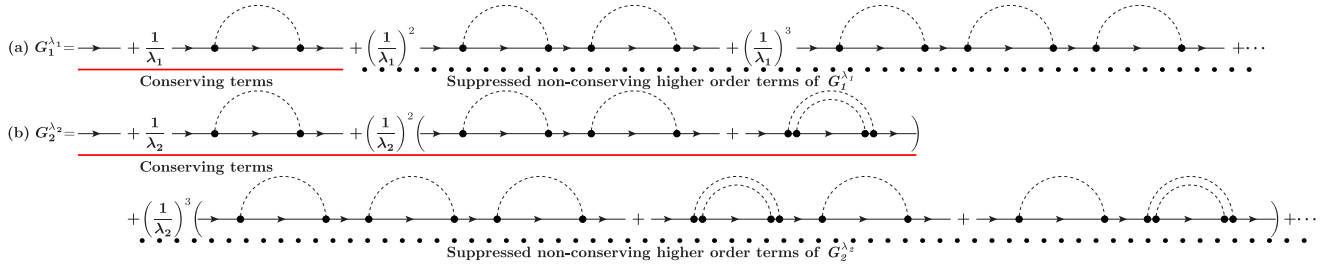$$

FIG. 2. Rescaled Green's functions, (a) $G_1^{\lambda_1}$ of first SCBA iteration and (b) $G_2^{\lambda_2}$ of second SCBA iteration, described by Feynman diagrams. Conserving and nonconserving terms are arranged in ascending order in interactions. Thin lines with an arrow indicate electron noninteracting Green's function. Dashed lines are for free phonon propagators.

Taking a relevant value of λ_1, the factors $(1/\lambda_1)^n$ $(n > 1)$ can eliminate the infinite sum of nonconserving terms while preserving the first-order conserving one. In NEGF, since any relevant expectation value $(\mathcal{O})$ is linear in the one-electron Green's function, the expectation value of the first-order term to G_{LOA1} can be constructed as $\Delta\mathcal{O}_1 = \mathcal{O}(g\Sigma[g]g) = \lambda_1[\mathcal{O}(G_1^{\lambda_1}) - \mathcal{O}(g)]$.

The same technique can be applied to the second SCBA iteration of Eq. (4) considering a different scaling factor λ_2 to obtain the rescaled G_2 as

$$G_2^{\lambda_2} = g + \frac{1}{\lambda_2}g\Sigma\big[G_1^{\lambda_2}\big]g$$
$$+ \left(\frac{1}{\lambda_2}\right)^2 g\Sigma\big[G_1^{\lambda_2}\big]g\Sigma\big[G_1^{\lambda_2}\big]g + \cdots, \qquad (8)$$

where $G_1^{\lambda_2}$ is G_1 rescaled by λ_2. Since the SCBA self-energy is linear with respect to the Green's function [33], the rescaled G_2 can be expressed as

$$G_2^{\lambda_2} = g + \frac{1}{\lambda_2}g\Sigma[g]g$$
$$+ \left(\frac{1}{\lambda_2}\right)^2 (g\Sigma[g]g\Sigma[g]g + g\Sigma[g\Sigma[g]g]g)$$
$$+ \left(\frac{1}{\lambda_2}\right)^3 (g\Sigma[g]g\Sigma[g]g\Sigma[g]g + \cdots) + \cdots, \qquad (9)$$

where λ_2 should be chosen to remove higher-order terms associated to $(1/\lambda_2)^n$ $(n > 2)$, but to maintain the first- and second-order conserving terms. With this scaling parameter, the expectation value of the second-order terms to second-order LOA Green's function G_{LOA2} can be obtained as $\Delta\mathcal{O}_2 = \mathcal{O}(g\Sigma[g]g\Sigma[g]g + g\Sigma[g\Sigma[g]g]g) = \lambda_2^2[\mathcal{O}(G_2^{\lambda_2}) - \mathcal{O}(g)] - \lambda_2\Delta\mathcal{O}_1$. Figures 2(a) and 2(b) illustrate this scaling technique in terms of Feynman diagrams for the first and second SCBA iterations, respectively.

Once the rescaled conserving Green's functions at each order are obtained, the expectation values of the desired observable can be reconstructed using the linearity property of the corresponding operator. In particular, Nth-order LOA current can be expressed as

$$\mathcal{I}_{N\text{thLOA}} = \mathcal{I}_0 + \sum_{n=1}^{N} \Delta\mathcal{I}_n, \qquad (10)$$

with

$$\Delta\mathcal{I}_N = (\lambda_N)^N \mathcal{I}_{N\text{thSCBA}}\big(G_N^{\lambda_N}\big) - \sum_{n=0}^{N-1} (\lambda_N)^{N-n}\Delta\mathcal{I}_n,$$
$$\Delta\mathcal{I}_0 = \mathcal{I}_0. \qquad (11)$$

This procedure demonstrates that conserving Green's function at any order N can be, in principle, obtained from conventional SCBA scheme. At each order N, λ_N has to be large enough to remove all nonconserving terms (whose order in interaction is larger than N) but small enough to maintain conserving terms (whose order in interaction is $\leqslant N$). This approach relies on the relevant choice of λ_N which can be rapidly verified through the current conservation. Explicitly we determine the λ_N's based on a semiempirical method noting that they are associated to a Taylor development of the Green's function. We first find the scaling parameter λ_1, which ensures that the current is conserved after the first SCBA iteration. We then deduce an approximated value of λ_2 as $2 \times (\lambda_1)^{1/2}$. Based on the same argument, we take λ_3 equal to $5 \times (\lambda_1)^{1/3}$. The multiplication factors 2 and 5 for λ_2 and λ_3, respectively, represent the weighting according to the number of diagrams at each order. We are aware of the empirical character of this approach, but the assessment of scaling parameters at any order in interactions and to any systems is a very complex issue out of the scope of the present work. Here, we calculate up to third-order currents and apply Padé approximants 0/1, 1/1, and 1/2. Calculation of higher-order LOA currents is also possible, but it usually requires additional SCBA iterations that could reduce the relevance of the presented technique. Moreover, the approach could have been also applied to the calculation of the charge-carrier density by using the same scaling parameters as those for the current. For the sake of clarity, we decided to only focus on the current considerations. The comparisons between SCBA and LOA/Padé approximant are performed with the same electrostatic potential profile as the one resulting from the self-consistent loop between the Poisson equation and the NEGF formalism including the interactions within the SCBA scheme.

Table I shows comparisons of the first three LOA orders and corresponding Padé currents with SCBA values for n-Si (n-type silicon) and n-Ge (n-type germanium) devices along several principal crystallographic orientations. We first see that all LOA current series (LOA1, LOA2, and LOA3) are diverging from SCBA currents, meaning that the considered devices operate in a relatively strong electron-phonon interaction

TABLE I. Comparisons of three first LOA currents and corresponding Padé approximants (0/1, 1/1, and 1/2) with the ballistic and SCBA currents in n-Si$\langle 100 \rangle$, n-Si$\langle 110 \rangle$, n-Si$\langle 111 \rangle$, and n-Ge$\langle 110 \rangle$ devices. Relative differences (ε) of the LOA and Padé currents with respect to the SCBA values are also reported ($\varepsilon = 100 \times |\mathcal{I}_{SCBA} - \mathcal{I}|/\mathcal{I}_{SCBA}$) where $\mathcal{I}$ is ballistic, LOA, or Padé current.

	Ballistic	LOA1	LOA2	LOA3	Padé 0/1	Padé 1/1	Padé 1/2	SCBA	Device
Current [A]	8.12×10^{-6}	6.40×10^{-6}	-2.37×10^{-5}	2.47×10^{-4}	6.70×10^{-6}	8.22×10^{-6}	5.05×10^{-6}	5.26×10^{-6}	n-Si$\langle 100 \rangle$
ε [%]	54.4	21.7	550.6	4595.8	27.4	56.3	4.0	0.0	
Current [A]	6.55×10^{-6}	4.58×10^{-6}	-3.92×10^{-5}	1.61×10^{-3}	5.04×10^{-6}	6.64×10^{-6}	4.42×10^{-6}	4.45×10^{-6}	n-Si$\langle 110 \rangle$
ε [%]	47.2	2.9	980.9	36079.8	13.3	49.2	0.7	0.0	
Current [A]	4.34×10^{-6}	1.72×10^{-5}	-4.38×10^{-5}	2.03×10^{-4}	-2.20×10^{-6}	6.59×10^{-6}	5.48×10^{-6}	6.01×10^{-6}	n-Si$\langle 111 \rangle$
ε [%]	27.8	186.2	828.8	3277.7	136.6	9.6	8.8	0.0	
Current [A]	5.27×10^{-6}	4.76×10^{-6}	2.09×10^{-6}	7.11×10^{-5}	4.80×10^{-6}	5.39×10^{-6}	4.72×10^{-6}	4.62×10^{-6}	n-Ge$\langle 110 \rangle$
ε [%]	14.1	3.0	54.8	1439.0	3.9	16.7	2.2	0.0	

regime [31]. Padé 0/1 applied to the first-order LOA currents shows an underestimation of the current degradation compared with the SCBA currents, except for the n-Si $\langle 111 \rangle$-oriented device. In addition, Padé 1/1 approximants based on up to second-order LOA currents are in most cases not reliable as pointed out in previous work [31]. However, the application of Padé 1/2 on the LOA current series shows significant improvements, with high accuracies compared with the SCBA values. For n-Si and n-Ge $\langle 110 \rangle$-oriented devices, Padé 1/2 provides almost the same values as the SCBA currents with a relative difference (ε) of less than 2% on average. It is also worth noting that Padé 1/2 can provide a reasonably good result ($<9\%$ relative difference) for the $\langle 111 \rangle$ transport direction where SCBA needs more than 40 iterations to converge. Therefore, currents resulting from Padé 1/2 can be seen as a good estimation of the SCBA values with a relative difference less than 10% for all the considered n-type devices. These results confirm the previous work [31] where it has been shown that Padé $N/N + 1$ can give better results even in strong electron-phonon interacting systems.

Table II shows similar results as Table I for p-type devices. We see that all LOA currents (LOA1, LOA2, and LOA3) are a divergent series like in the case of n-type devices. Table II also reports very favorable results for the $\langle 110 \rangle$ direction for which even the simplest Padé 0/1 guarantees a high agreement of the current ($\varepsilon < 6\%$) with respect to the SCBA approach. Padé 1/1 also produces reliable results for the $\langle 110 \rangle$ direction while remaining unstable for the other configurations. Padé 1/2 still gives current value very close to those of SCBA with ε less than

6%. The result is also remarkable for the $\langle 100 \rangle$ direction where Padé 1/2 provides similar accuracy while SCBA requires more than 80 iterations. However, the comparison is less successful for the p-Si$\langle 111 \rangle$ configuration for which all LOA and Padé currents fail to reproduce the SCBA result.

The transport along the $\langle 111 \rangle$ direction is quite singular for both n-type and p-type devices. For that orientation first-order LOA currents are larger than the ballistic values (see Tables I and II). Concerning the n-type device, the converged SCBA current is also larger than the ballistic one and the Padé 1/2 finally succeeds in providing an accurate value. In n-type $\langle 111 \rangle$-oriented NWs the counterintuitive increase of the current in the presence of phonon scattering with respect to the ballistic value results from the interplay between two competing effects: first, backscattering caused by phonon emission or absorption tends to decrease the current magnitude. Second, intersubband scattering induced by electron-phonon interactions connects bands with a small energy bandwidth that would otherwise not carry any current in the ballistic limit of transport [45,46]. In ultrashort devices with band structure exhibiting several subbands with a low energy bandwidth, as $\langle 111 \rangle$-oriented Si nanowires, the second effect dominates, thus leading to an increase of the current. However, in longer devices, backscattering plays the major role and the situation goes back to normal, i.e., the current magnitude decreases when electron-phonon scattering is turned on. The case of the p-type device is more pathological since the converged SCBA becomes smaller than the ballistic value. Such a configuration seems to involve more complex physical

TABLE II. Comparisons of three first LOA currents and corresponding Padé approximants (0/1, 1/1, and 1/2) with the ballistic and SCBA currents in p-Si$\langle 100 \rangle$, p-Si$\langle 110 \rangle$, p-Si$\langle 111 \rangle$, and p-Ge$\langle 110 \rangle$ devices. Relative differences (ε) of the LOA and Padé currents with respect to the SCBA values are also reported ($\varepsilon = 100 \times |\mathcal{I}_{SCBA} - \mathcal{I}|/\mathcal{I}_{SCBA}$) where $\mathcal{I}$ is ballistic, LOA, or Padé current.

	Ballistic	LOA1	LOA2	LOA3	Padé 0/1	Padé 1/1	Padé 1/2	SCBA	Device
Current [A]	6.10×10^{-6}	1.96×10^{-6}	3.53×10^{-8}	-3.36×10^{-5}	3.63×10^{-6}	-1.65×10^{-6}	3.89×10^{-6}	4.31×10^{-6}	p-Si$\langle 100 \rangle$
ε [%]	41.5	54.5	99.2	879.6	15.8	138.3	9.7	0.0	
Current [A]	6.26×10^{-6}	3.77×10^{-6}	5.07×10^{-6}	1.81×10^{-5}	4.48×10^{-6}	4.66×10^{-6}	4.48×10^{-6}	4.74×10^{-6}	p-Si$\langle 110 \rangle$
ε [%]	32.1	20.5	7.0	281.9	5.5	1.7	5.5	0.0	
Current [A]	5.29×10^{-6}	8.18×10^{-6}	-4.12×10^{-5}	3.70×10^{-3}	1.16×10^{-5}	5.45×10^{-6}	9.08×10^{-6}	4.85×10^{-6}	p-Si$\langle 111 \rangle$
ε [%]	9.1	68.7	949.5	76188.7	139.2	12.4	87.2	0.0	
Current [A]	5.80×10^{-6}	4.11×10^{-6}	4.70×10^{-6}	5.03×10^{-7}	4.49×10^{-6}	4.55×10^{-6}	4.49×10^{-6}	4.74×10^{-6}	p-Ge$\langle 110 \rangle$
ε [%]	22.4	13.3	0.8	89.4	5.3	4.0	5.3	0.0	

phenomena that require one to consider higher-order LOA currents. It clearly illustrates the limit of our technique to reproduce SCBA currents. We also mention that it has been recently shown [47,48] that the SCBA with Luttinger-Ward functional self-energy may produce unphysical convergence for strong-coupling systems. The $\langle 111 \rangle$ p-type direction could be one of these configurations. We can also note that a similar approach using hypergeometric resummation has been recently proposed and could be tested in such case [49]. However, we suggest one take as a warning signal of the accuracy of the present approach the situation where first-order LOA current is larger than the ballistic one.

In summary, we have proposed a numerically efficient technique to reproduce the SCBA currents. It relies on the LOA coupled to Padé approximants and only requires the first few iterations of the SCBA procedure. The method has been applied to NW transistors using an atomistic 3D quantum transport code. We focused on the saturation regime current of the devices at high gate bias and compared the LOA and Padé currents with the SCBA values. In particular, we showed that the Padé 1/2 with only first three-order LOA currents can successfully reproduce the SCBA currents with a small relative difference ($<$10%) in most of the considered devices except for the p-Si$\langle 111 \rangle$ device where the electron-phonon interaction exhibits singular effects. We also suggested as a warning signal to SCBA solution the case where first-order LOA current is larger than the ballistic one.

[1] Intel 22nm 3-d tri-gate transistor technology, May 2, 2011, https://newsroom.intel.com/press-kits/intel-22nm-3-d-tri-gate-transistor-technology (Date of access: 17/05/2017).

[2] H. Mertens *et al.*, Gate-all-around MOSFETs based on vertically stacked horizontal Si nanowires in a replacement metal gate process on bulk Si substrates, *2016 IEEE Symposium on VLSI Technology, Honolulu, HI* (IEEE, New York, 2016), pp. 1–2.

[3] L. Li, Y. Yu, G. J. Ye, Q. Ge, X. Ou, H. Wu, D. Feng, X. H. Chen, and Y. Zhang, Nat. Nanotechnol. **9**, 372 (2014).

[4] A. D. Franklin, M. Luisier, S.-J. Han, G. Tulevski, C. M. Breslin, L. Gignac, M. S. Lundstrom, and W. Haensch, Nano Lett. **12**, 758 (2012).

[5] B. Radisavljevic, A. Radenovic, J. Brivio, V. Giacometti, and A. Kis, Nat. Nanotechnol. **6**, 147 (2011).

[6] Y. Yoon, K. Ganapathi, and S. Salahuddin, Nano Lett. **11**, 3768 (2011).

[7] A. Szabó, R. Rhyner, and M. Luisier, Phys. Rev. B **92**, 035435 (2015).

[8] J. Cao, D. Logoteta, S. Özkaya, B. Biel, A. Cresti, M. G. Pala, and D. Esseni, IEEE Trans. Electron Devices **63**, 4388 (2016).

[9] K. Tomioka, M. Yoshimura, and T. Fukui, Nature (London) **488**, 189 (2012).

[10] L.-F. Shen, S. Yip, Z. Yang, M. Fang, T. Hung, E. Y. B. Pun, and J. C. Ho, Sci. Rep. **5**, 16871 (2015).

[11] X. Zhou *et al.*, Scalability of InGaAs gate-all-around FET integrated on 300mm Si platform: Demonstration of channel width down to 7nm and Lg down to 36nm, *2016 IEEE Symposium on VLSI Technology, Honolulu, HI* (IEEE, New York, 2016), pp. 1–2.

[12] M. Di Ventra, S. T. Pantelides, and N. D. Lang, Phys. Rev. Lett. **84**, 979 (2000).

[13] S. Poli, M. G. Pala, T. Poiroux, S. Deleonibus, and G. Baccarani, IEEE Trans. Electron Devices **55**, 2968 (2008).

[14] H. Carrillo-Nuñez, M. Bescond, N. Cavassilas, E. Dib, and M. Lannoo, J. Appl. Phys. **116**, 164505 (2014).

[15] H. M. Yann-Michel Niquet and C. Delerue, Appl. Phys. Lett. **100**, 153119 (2012).

[16] M. Kobayashi and T. Hiramoto, J. Appl. Phys. **103**, 053709 (2008).

[17] X. Zhao, C. M. Wei, L. Yang, and M. Y. Chou, Phys. Rev. Lett. **92**, 236805 (2004).

[18] G. Pizzi, M. Gibertini, E. Dib, N. Marzari, G. Iannaccone, and G. Fiori, Nat. Commun. **7**, 12585 (2016).

[19] M. Moussavou, N. Cavassilas, E. Dib, and M. Bescond, J. Appl. Phys. **118**, 114503 (2015).

[20] A. Lherbier, M. P. Persson, Y.-M. Niquet, F. Triozon, and S. Roche, Phys. Rev. B **77**, 085301 (2008).

[21] M. Luisier and G. Klimeck, Phys. Rev. B **80**, 155430 (2009).

[22] F. Murphy-Armando, G. Fagas, and J. C. Greer, Nano Lett. **10**, 869 (2010).

[23] S. Datta, *Electronic Transport in Mesoscopic Systems* (Cambridge University Press, Cambridge, UK, 1995).

[24] D. K. Ferry and S. M. Goodnick, *Transport in Nanostructures* (Cambridge University Press, Cambridge, UK, 1997).

[25] H. Haug and A.-P. Jauho, *Quantum Kinetics in Transport and Optics of Semiconductors,* Springer Series in Solid-State Sciences Vol. 123 (Springer, Berlin, 1996).

[26] A. Svizhenko, M. P. Anantram, T. R. Govindan, B. Biegel, and R. Venugopal, J. Appl. Phys. **91**, 2343 (2002).

[27] S. Jin, Y. J. Park, and H. S. Min, J. Appl. Phys. **99**, 123719 (2006).

[28] G. Mil'nikov and N. Mori, J. Comput. Electron. **15**, 1179 (2016).

[29] R. Rhyner and M. Luisier, Phys. Rev. B **89**, 235311 (2014).

[30] R. Rhyner and M. Luisier, Nano Lett. **16**, 1022 (2016).

[31] Y. Lee, M. Lannoo, N. Cavassilas, M. Luisier, and M. Bescond, Phys. Rev. B **93**, 205411 (2016).

[32] H. Mera, M. Lannoo, C. Li, N. Cavassilas, and M. Bescond, Phys. Rev. B **86**, 161404 (2012).

[33] H. Mera, M. Lannoo, N. Cavassilas, and M. Bescond, Phys. Rev. B **88**, 075147 (2013).

[34] G. H. Hardy, *Divergent Series* (Chelsea, New York, 1991).

[35] J. G. A. Baker and P. Graves-Morris, *Padé Approximants* (Cambridge University Press, Cambridge, 1996).

[36] J. C. Slater and G. F. Koster, Phys. Rev. **94**, 1498 (1954).

[37] T. B. Boykin, G. Klimeck, and F. Oyafuso, Phys. Rev. B **69**, 115201 (2004).

[38] S. Lee, F. Oyafuso, P. von Allmen, and G. Klimeck, Phys. Rev. B **69**, 045316 (2004).

[39] Z. Sui and I. P. Herman, Phys. Rev. B **48**, 17938 (1993).

[40] A. Paul, M. Luisier, and G. Klimeck, J. Comput. Electron. **9**, 160 (2010).

[41] T. Kubis and P. Vogl, J. Comput. Electron. **6**, 183 (2007).

[42] N. Cavassilas, F. Michelini, and M. Bescond, J. Comput. Electron. **15**, 1233 (2016).

[43] R. Rhyner and M. Luisier, J. Appl. Phys. **114**, 223708 (2013).

[44] G. D. Mahan, *Many-Particle Physics* (Plenum, New York, 1990).

[45] J. Chang, L. F. Register, and S. K. Banerjee, Appl. Phys. Lett. **103**, 223509 (2013).

[46] A. Szabó, Dissipative quantum transport simulations in two-dimensional semiconductor devices from first principles, Ph.D. thesis, ETH Zurich, 2016 .

[47] W. Lee, N. Jean, and S. Sanvito, Phys. Rev. B **79**, 085120 (2009).

[48] A. Stan, P. Romaniello, S. Rigamonti, L. Reining, and J. A. Berger, New J. Phys **17**, 093045 (2015).

[49] H. Mera, T. G. Pedersen, and B. K. Nikolić, Phys. Rev. B **94**, 165429 (2016).